Estuarine, Coastal and Shelf Science 237 (2020) 106628

Contents lists available at ScienceDirect

Estuarine, Coastal and Shelf Science

journal homepage: http://www.elsevier.com/locate/ecss

Assessment of Ba/Ca in *Arctica islandica* shells as a proxy for phytoplankton dynamics in the Northwestern Atlantic Ocean

Justine Doré [a,*], Gwénaëlle Chaillou [b], Pierre Poitevin [a], Pascal Lazure [c], André Poirier [d], Laurent Chauvaud [a], Philippe Archambault [e], Julien Thébault [a,**]

[a] Univ Brest, CNRS, IRD, Ifremer, LEMAR, Plouzané, France
[b] Canada Research Chair in Geochemistry of Coastal Hydrogeosystems, Québec-Océan, ISMER, UQAR, Rimouski, Canada
[c] Ifremer, Univ Brest, CNRS, IRD, LEMAR, Plouzané, France
[d] GEOTOP and Département des Sciences de la Terre et de l'atmosphère, UQAM, Montréal, Canada
[e] Québec Océan, Département de Biologie, Université Laval, Québec, QC, Canada

ARTICLE INFO

Keywords:
A. islandica
Ba/Ca
Master chronology
Cross-dating
Chlorophyll *a*
Northwestern Atlantic

ABSTRACT

Despite its major role as a global climate regulator, little is known about the recent evolution of the North Atlantic Ocean, especially prior to the fifties, principally because of the lack of long-term instrumental data. Moreover, the North Atlantic Ocean is undergoing rapid changes at the physical scale leading to modifications at the biological scale increasing interest to monitor the environment. The phytoplankton is the base of the ocean life and its perturbation can lead to further changes in the food chain. Recording its dynamics implies to observe both its spatial and temporal variations. This study brings forward the use of the Ba/Ca ratio from shells of the long-living bivalve *Arctica islandica* collected in the Northwestern Atlantic Ocean near Saint-Pierre and Miquelon (SPM) as a recorder of the past and present phytoplankton dynamics. A high inter and intra-reproducibility and synchrony between Ba/Ca_{shell} profiles were demonstrated allowing the reconstruction of a 124 years annually-resolved Ba/Ca_{shell} master chronology (from 1893 to 2016). This master chronology was positively correlated to the surface chlorophyll *a* measured by satellite sensor at regional (around SPM) and global scales (Northwestern Atlantic).

1. Introduction

The North Atlantic Ocean, particularly the northwest corner, has been the focus of much attention in recent years because it plays a major role in the Meridional Overturning Circulation (Lozier, 2012) and more especially because of the physical changes it has undergone (i.e., weakening of the Atlantic Meridional Overturning Circulation (AMOC); Smeed et al., 2014; Rahmstorf et al., 2015) since the mid-1920s, due to increases of anthropogenic CO_2 (Caesar et al., 2018). This weakening could be caused by a poleward retreat of the Labrador Current, a warming of the Gulf Stream region, and/or a cooling of the subpolar gyre region due to a northward shift of the Gulf Stream and reduced heat transport (Saba et al., 2016; Caesar et al., 2018). Several studies (Han and Tang, 2001; Häkkinen and Rhines, 2004; Han et al., 2010) have indicated that the weakening of AMOC in the 1990s was related to strong changes in atmospheric variability in the North Atlantic Ocean, where the dominant climate-driven mode is the North Atlantic Oscillation (NAO) (Hurrell and Deser, 2010). These physical changes may lead to biological changes such as a decrease in global primary production and in the sinking velocity of particulate organic carbon (Steinacher et al., 2010) as well as a shift in phytoplankton communities (Marinov et al., 2010; Harrison et al., 2013), with major impacts on the energy fluxes between phytoplankton and higher trophic levels (Stock et al., 2014).

The increasing interest in primary production has brought about the development of new tools to measure chlorophyll *a* (Chl *a*) concentration as a proxy for phytoplankton abundance. However, such measurements are sparse and exist only for recent years. For example, even though satellite ocean colour sensors are currently useful for evaluating the spatio-temporal dynamics of global marine phytoplankton, these instruments have only been recording since 1978 (e.g., CZCS sensor; Hovis et al., 1980) thus there are less than four decades of Chl *a* records.

* Corresponding author.
** Corresponding author.
E-mail addresses: justine.dore@univ-brest.fr (J. Doré), julien.thebault@univ-brest.fr (J. Thébault).

https://doi.org/10.1016/j.ecss.2020.106628
Received 13 December 2019; Received in revised form 29 January 2020; Accepted 3 February 2020
Available online 7 February 2020

Since then, numerous ocean colour satellite sensors have been deployed (e.g. SeaWiFS, MERIS, MODIS-Aqua, VIIRS; see Emberton et al. 2015 and references therein) to study phytoplankton dynamics. However, contradictory results have been reported on the way global ocean chlorophyll has changed over the last century (Gregg, 2005; Boyce et al., 2010; Feng and Zhu, 2012), and global trends may not be in line with regional or local trends, where variations can be opposite (EEA, 2005). In this context, it is crucial to find new tools and methods to accurately quantify trends in marine phytoplankton dynamics at a defined location.

Very recently, some studies pointed out an influence of primary production in the Northeast Atlantic on growth rates of the long-lived bivalve *Arctica islandica* (Ballesta-Artero et al., 2018; Bonitz et al., 2018; Poitevin et al., 2019). Variations of shell growth rates were positively correlated to the local and regional intensity of primary production. This phenomenon is attributed to the algal food-availability: concentration of algal food, therefore intensity of primary production, drives shell growth. Poitevin et al. (2019) reported a similar relationship with the local primary production near Saint-Pierre and Miquelon (south of Newfoundland in the NW Atlantic) that might be influenced by regional to global hydrographic (e.g., temperature, oceanography) and climatic (e.g., NAO, Atlantic Multi-decadal Oscillation) phenomena. Considering the findings of this last study, it would be interesting to further explore this relationship using another specific proxy that is potentially linked to primary production.

For several decades, past and present primary production levels have been reconstructed using an array of biological and geochemical proxies archived in sediment (Dymond et al., 1992; Seki et al., 2004; Chmura et al., 2004; Genovesi et al., 2011). Muzuka and Hillaire-Marcel (1999) showed the influence of the Western Boundary Undercurrent in the Labrador Sea (Northwestern Atlantic Ocean) on the sedimentation rate of organic matter (from primary production), but on the scale of millennia. To deal with the problem of low temporal resolution of sediment cores (generally more than a decade), several biogenic archives have been investigated, e.g., foraminifera (see Katz et al., 2010, for review), corals (see Lea, 2014, for review) and, more recently, bivalves (see Prendergast et al., 2017, for review). This latter archive allows the reconstruction of paleo-productivity because bivalves offer precise and high temporal resolution (sub-daily to annual; Rhoads and Pannella, 1970). Shell growth occurs by periodic accretion of calcium carbonate layers. When the calcification pattern is well known, accurate formation dates can be estimated for each growth increment. Several minor and trace elements incorporated during shell calcification are also used as environmental proxies (e.g., Mg, Sr, Mn, Ba). Unlike corals and foraminifera, the strong biological control on the incorporation of these elements into the shell matrix makes interpretation of the elemental footprint difficult (Rosenberg, 1989; Purton et al., 1999; Gillikin et al., 2005; Lorrain et al., 2005; Carré et al., 2006; Takesue et al., 2008). Nevertheless, many studies have highlighted the potential of the Ba/Ca_{shell} ratio as an environmental proxy for primary production and phytoplankton dynamics (Stecher et al., 1996; Vander Vander Putten et al., 2000; Lazareth et al., 2003; Thébault et al., 2009; Hatch et al., 2013; Marali et al., 2017a,b). Temporal variations in the Ba/Ca_{shell} ratio along the shell growth axis are characterized by a low, relatively constant background interrupted by sharp peaks that are often synchronous between contemporaneous specimens from the same locality. Stecher et al. (1996) first related these peaks to phytoplankton blooms, suggesting that after a bloom, organic-rich decaying phytoplankton flocs lead to the formation of barite ($BaSO_4$) crystals (Dehairs et al., 1980; Bishop, 1988). However, it is still unclear if these Ba/Ca_{shell} peaks are directly due to ingestion of Ba-rich phytoplankton or indirectly by intake of $BaSO_4$.

Here, we investigated temporal variations in the Ba/Ca_{shell} ratio in previously studied *Arctica islandica* (Linnaeus, 1767) shells collected in Saint-Pierre and Miquelon (SPM) (Poitevin et al., 2019). Located at the boundary between the cold Labrador current (LC) and the warm Gulf Stream (GS) waters, this archipelago is an excellent site to capture changes in the climate and oceanography of the North Atlantic. Much attention has been paid to this bivalve mollusc, in particular because of its exceptional lifespan (maximum of 507 years recorded to date; Butler et al., 2013) and its status as one of the most effective archives for reconstructing marine environments and regional climate before instrumental data were available (see Schöne, 2013, for a review). However, only a few studies (Schöne et al., 2013; Marali et al., 2017b) have examined the potential of skeletal barium as an environmental proxy and none of them focused on populations from the Northwestern Atlantic.

The objective of this study was to explore the dynamics of primary production and phytoplankton in the Northwestern Atlantic Ocean by coupling sclerochronological and geochemical approaches developed on a long-living bivalve, *Arctica islandica*. More specifically, we aimed (i) to test the methodology and propose a robust master chronology of the Ba/Ca_{shell} ratio covering the longest possible time period, and (ii) to assess the potential of the Ba/Ca_{shell} ratio as a cross-dating tool and as an environmental proxy. For the first point, we used the Ba/Ca_{shell} ratio instead of only age to cross-date contemporaneous specimens, for the second point, we compared geochemical data with remote sensing results. Finally, based on the results reported by Poitevin et al. (2019), we proposed (iii) to discuss phytoplankton dynamics in the Northwestern Atlantic where, according to our knowledge, this *Arctica islandica* master chronology of Ba/Ca_{shell} ratio is the northernmost and shallowest of this region. It represents a unique opportunity to elucidate the relationship between bivalves shell growth and multi-scale oceanographic parameters.

2. Methods

2.1. Study site

The French archipelago of Saint-Pierre and Miquelon is located off the southern coast of Newfoundland (NFL) near Cabot Strait (Fig. 1A and B). The oceanographic conditions in this region are influenced by the seasonality of the inshore and offshore branches of the Labrador Current (Han, 2005; Han et al., 2008). Specimens of *A. islandica* were collected close to the southeastern shore of the Miquelon-Langlade isthmus (46°54′08″N; 56°17′26″W) (Fig. 1C). All specimens were sampled alive by SCUBA divers at 14–15 m in depth on a sandy substrate in September 2016, September 2017, and July 2018 (Table 1). In addition, a dead, well preserved, shell was also collected at the same location in July 2018.

2.2. Preparation of shells

For all live-collected specimens, the soft tissues were removed shortly after collection. Shells were carefully cleaned with freshwater to remove sediment and remaining soft tissues and then air-dried. The left valve of each specimen was selected for all analyses except for specimen A140916, for which both valves were analyzed. The shell was covered from the umbo to the ventral margin along the axis of maximum growth with a thick, 1 cm wide layer of quick-drying metal epoxy resin (Araldite Metal, Huntsman Advanced Materials) to protect the shell from breaks during sectioning. Two 1 mm thick radial cross-sections ("mirror" cross-sections) were then cut along the axis of maximum growth using a low-speed precision saw (Struers, Secotom-10; rotation speed 500 rpm; feed speed 200 μm s^{-1}) equipped with a 600 μm thick diamond-coated blade continuously cooled by water. Both sections were glued onto glass slides, ground with 1200 then 2500 grit wet-table carborundum paper, then polished with a polishing cloth and a 1 μm diamond liquid (Escil) on a grinding turntable (Struers, TegraPol-25). To remove residual diamond liquid and/or abrasive material, cross-sections were cleaned with deionized water and dried between each grinding/polishing step to reduce scratches and the chance of contamination. One of the two mirror cross-sections was used to study growth rate and the other for

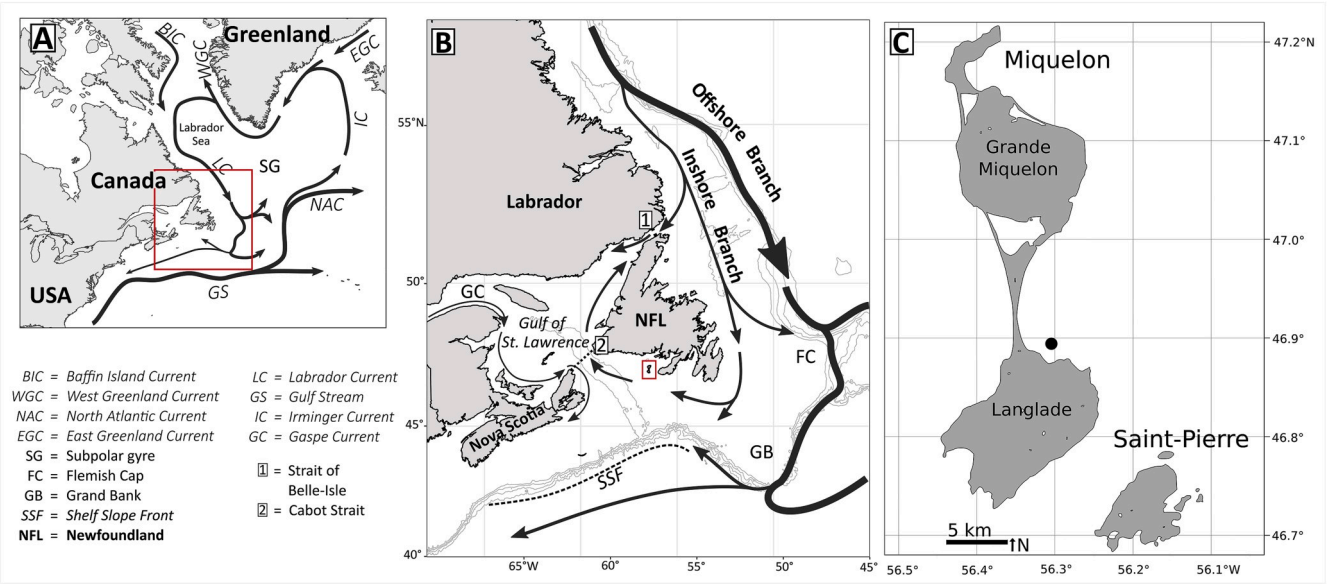

Fig. 1. Location of the Saint-Pierre and Miquelon Archipelago in the Northwestern Atlantic Ocean. (A) Major oceanographic surface currents. (B) Overview map of the inshore (thin line) and offshore (thick line) branches of the Labrador Current around the sampling area (red box). (C) Detailed map of the SPM archipelago. Black dot indicates the sampling site. (For interpretation of the references to colour in this figure legend, the reader is referred to the Web version of this article.)

Table 1
Summary of shells used in this study: shell ID, hatch, year of death, age (y), and collection date. Asterisks indicate shells used in Poitevin et al. (2019).

Shell ID	Hatch	Death	Age	Sampling date
A030718	1959	2004	44	July 2018
A040916*	1892	2016	122	September 2016
A050718	1953	2018	63	July 2018
A060916	1972	2016	42	September 2016
A100916*	1955	2016	59	September 2016
A140917	1900	2017	115	September 2017
A140916*	1928	2016	86	September 2016
A210916*	1902	2016	112	September 2016
A250916*	1923	2016	91	September 2016
A690916	1971	2016	43	September 2016
A710916	1970	2016	44	September 2016
A890916*	1945	2016	69	September 2016
A1050916*	1913	2016	101	September 2016
A1100916*	1959	2016	55	September 2016

geochemical analyses (Fig. 2A).

2.3. Sclerochronological analysis

A standardized growth indices (SGI) master chronology based on 32 specimens of *A. islandica* collected in 2016 was presented in Poitevin et al. (2019). For this study, we enhanced this database by adding six individuals collected at the same location in 2017 and 2018. Construction of the chronology is described in Poitevin et al. (2019); here, we only present the method used to complete the master chronology. Briefly, to age specimens, shell cross-sections were immersed in Mutvei's solution (Schöne et al., 2005) for 1 h at ambient temperature to improve visualization of annual growth lines. After gentle rinsing and drying, stained cross-sections were observed under reflected light (Zeiss, KL 2500 LCD). Digital images were taken with an AxioCam MRc5 installed on a Zeiss Lumar.V12 stereomicroscope equipped with a motorized stage (30x magnification), and then processed with ImageJ software to measure annual increment width. Age determination was made in the OSL for all specimens, as presented by Poitevin et al. (2019). Several specimens were then selected as a function of their age for the purpose of this study.

2.4. Geochemical analyses

Fourteen specimens were analyzed with a Nu Attom high-resolution inductively coupled plasma mass spectrometer (HR-ICP-MS) coupled to a Photon-Machines G2 laser ablation system (noted LA-ICP-MS thereafter) at the Research Centre on the Dynamics of the Earth System (GEOTOP), *Université du Québec à Montréal (UQAM)*). Chemical element analysis was performed in line scan mode along the maximum growth axis. Prior to analysis, shell cross-sections were pre-ablated (to generate a clean surface) using a spot diameter of 150 µm and a scan speed 100 µm s^{-1}. The analysis was performed using a spot diameter of 65 µm and a scan speed of 10 µm s^{-1}. Measurements were acquired every 0.41 s, corresponding to an integrated step of around 5 µm. During acquisition, signal intensities were recorded for ^{135}Ba and ^{43}Ca. The intensity of ^{135}Ba was systematically normalized against the ^{43}Ca signal (internal standard) to correct for laser beam energy drift, focus variation at the sample surface, and ICP-MS detection drift. The glass reference material NIST SRM 612 was used as a calibration standard whereas NIST SRM 614 was analyzed to check the calibration (Jochum et al., 2011). Data processing (including instrumental drift correction and normalization) was performed using the IOLITE (https://iolite-software.com/) package (Hellstrom et al., 2008; Paton et al., 2011) which operates within Igor Pro (http://www.wavemetrics.com). Ba/Ca_{shell} ratios are expressed in µmol.mol^{-1}.

2.5. Ba/Ca_{shell} ratio time series

Measurements of the Ba/Ca_{shell} ratio were performed using one of two methods, depending on the age of the shell. For each shell aged less than 50 years, the whole HP and the last 1/3 of the OSL were analyzed. For older specimens (>50 years), analyses were restricted to the first 2/3 of HP (i.e., around 25 years of growth; Fig. 2B).

To allow a better comparison between Ba/Ca_{shell} ratios of different annual increments and different shells, each signal was resampled to remove the ontogenetic effect, so that each sample represented the same amount of time. Because growth rate decreases with age, the number of data points per annual increment also decreases towards the ventral margin when the spot size is kept constant (65 µm), resulting in variable temporal resolution along the shell growth axis. To circumvent this issue, Ba/Ca_{shell} measurements were separated using shell growth

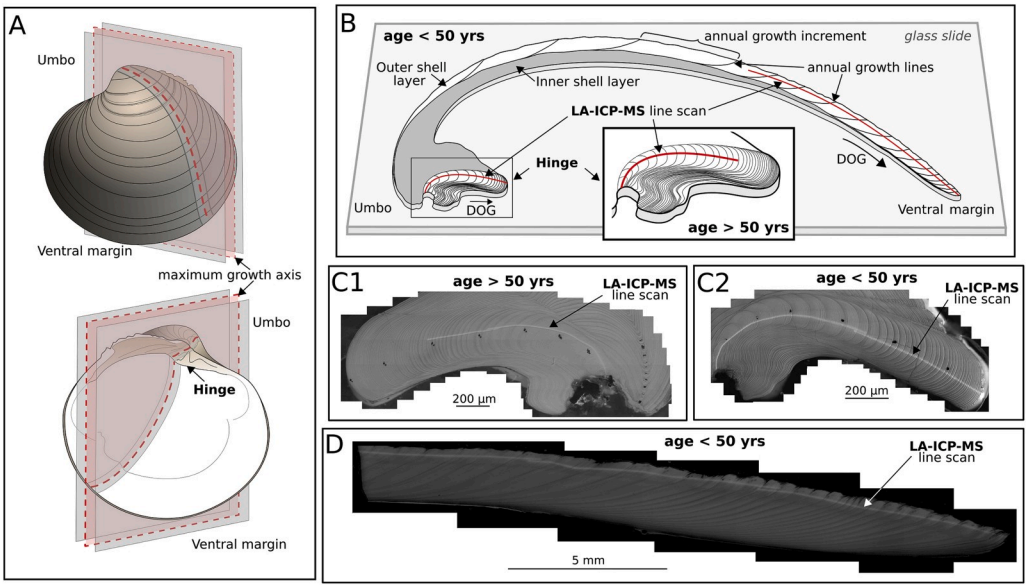

Fig. 2. (A) Representation of the three different cut axes selected to produce two mirror cross-sections, one used for sclerochronology and the other for geochemical analyses. Red dashed lines indicate the maximum growth axis on which growth increment width measurements and geochemical analyses were performed. (B) Drawing of a shell cross-section along the maximum growth axis. Red lines represent the LA-ICP-MS line scans. Only the first two thirds of the hinge plate (HP) were analyzed in specimens older than 50 years old. For specimens less than 50 years old, the whole HP was analyzed along the maximum growth axis, along with the last third of the outer shell layer (OSL). (C1) Image of the HP of an old specimen (shell ID A250916, Table 1). (C2) Image of the HP of a young specimen (shell ID A710916, Table 1). (D) Image of the ontogenetically older portion of the OSL of a young specimen. (For interpretation of the references to colour in this figure legend, the reader is referred to the Web version of this article.)

increments as a calendar dates and then fitted with a cubic spline; the curve was re-sampled so that 50 data points were available for each annual increment for all shells. Re-sampling was performed using the AnalySeries software version 2.0.4 (Paillard et al., 1996). Each Ba/Ca_{shell} ratio was then smoothed using a running mean of 10 points. To avoid possible signal contamination *via* metal epoxy or glue, the first and last years of each sample were removed from the dataset.

2.5.1. Intra- and inter-individual reproducibility

To create a robust inter-individual overlapped Ba/Ca record, thereafter called master chronology, the reproducibility of the Ba/Ca_{shell} ratio was tested using two strategies. First, the Ba/Ca_{shell} signal from the left valve HP was compared to the right valve HP for the same specimen (shell A140916; Table 1). Second, the Ba/Ca_{shell} ratio of shell A710916 was analyzed in both the HP and OSL from the right valve. Furthermore, to assess the synchrony between inter-shell Ba/Ca_{shell} values, HPs were selected according to their age so that there were overlaps of more than two years between samples. To easily compare inter-shell signals, the temporal alignment was done by re-sampling fifty-points-a-year signals as explained above (i.e., signals from the same year can be easily compared with each other). We assumed here that each point from the re-sampled signals from a same individual represents exactly the same calcification duration, thus parts of a same shell theoretically have the same growth speed.

2.5.2. Construction of the Ba/Ca_{shell} master chronology

We selected the HP because it is well preserved: compared to the OSL, it does not undergo attacks by euendoliths or erosion, and it is also less fragile. Some specimens previously analyzed for shell growth patterns by Poitevin et al. (2019) were selected according to their ages to get the longest continuous record of Ba/Ca_{shell} (Table 1). To obtain the best temporal resolution, only the first 10–25 years of life were analyzed for the Ba/Ca_{shell} ratio, except for younger specimens (Fig. 2), and then assembled with a minimum overlap of two years. To fill some gaps in this record, two additional specimens collected in July 2018 were also analyzed.

To construct the master chronology, the mean per year of the maximum Ba/Ca per specimen was calculated to obtain a annually-resolved Ba/Ca_{shell} master chronology (Table 1). In addition, the synchrony of the maximum Ba/Ca_{shell} per year per individual was tested to assess the statistical robustness of the master chronology. To test the potential of Ba/Ca as a cross-dating tool, the "leave-one-out" principle was applied: one sample was removed from the data set ranked by age, and this sample with an assumed unknown hatch date was reinserted where the correlation between the Ba/Ca signal and the data set was the best. A hatch date was then obtained and compared to the actual one.

2.6. Instrumental data

The Ba/Ca_{shell} ratio has often been considered to be influenced by an environmental driver, although what this could be is not clear. Here, we focused our effort on the link between the Ba/Ca_{shell} ratio record and phytoplankton dynamics because several studies have proposed this hypothesis (Stecher et al., 1996; Vander Putten et al., 2000; Lazareth et al., 2003; Thébault et al., 2009; Hatch et al., 2013; Marali et al., 2017b). We focused on satellite Chl *a* measurements because no *in-situ* Chl *a* data are available for the sampling area. We used data from the Ocean GlobColour web site (http://hermes.acri.fr/) between 1998 and 2016 that have a monthly resolution. Two areas of interest were selected: Northwestern Atlantic (40–66°N, 40–60°W) and a smaller rectangle containing our study site (47°18′45″N-46°36′14.976″N, 56°03′44.999″W-56°38′44.987″W), referred to here as the local scale. Annually-resolved Ba/Ca_{shell} values from our master chronology were compared with monthly Chl *a* data.

Poitevin et al. (2019) showed that the growth rate of *A. islandica* from the Northwestern Atlantic is linked to climate variations such as the NAO. Furthermore, they highlighted a correlation between the growth rate of SPM *A. islandica* and local Chl *a* concentration measured by satellite sensors which may be linked to ocean decadal oscillations. Thus, to see if Ba/Ca is a potential proxy for phytoplankton dynamics, our Ba/Ca_{shell} master chronology was compared with annual mean values of decadal and multi-decadal time-scale climatic indices: the NAO (Hurrell and Deser, 2010) and the AMO (Schlesinger and Ramankutty, 1994). NAO data were extracted from the Climatic Research Unit (University of East Anglia, UK), and annual AMO data were extracted from the NOAA Earth System Research Laboratory (USA).

2.7. Statistical analysis

To assess the reproducibility and the synchrony between individual signals of Ba/Ca_{shell}, a linear regression was used to calculate the coefficient of determination with an associated *p*-value. The correlation coefficient was calculated using the Pearson's product-moment correlation on a 10-point running mean. A pairwise matrix correlation was calculated from the annual maximum values of Ba/Ca_{shell} from each shell with a common growth period. Robustness of the Ba/Ca_{shell} master chronology was assessed through calculation of EPS (Expressed Population Signal) using the dplR package (https://CRAN.R-project.org/package=dplR). Correlation coefficients were calculated between the annually-resolved Ba/Ca_{shell} master chronology, the different ocean oscillation indices, and the Chl *a* concentration from the two selected areas. Spatial correlation maps were produced to visualize the significant correlation between the master chronology and monthly Chl *a* measured by satellite sensors from the selected Northwestern Atlantic area.

3. Results

The Ba/Ca_{shell} time-series show a flat background interrupted by sharp peaks (Figs. 3–5). Peaks (1 or 2 per year) usually appear in the first half of the growth increment, sometimes right after a growth line. However, some increments do not show any peaks. Unless specified, all results specific to Ba/Ca_{shell} signals arise from the calculation of a 10-point running mean.

3.1. Intra-individual Ba/Ca_{shell} time series reproducibility

The Ba/Ca_{shell} ratio measured from the same individual from two different parts (right vs. left valves or HP vs. OSL) show similar contemporaneous variations (Figs. 3–4). HP analyses of shell A140916 revealed that the left valve record did not go back as far as the right one (1931 and 1929, respectively) (Fig. 3). Signals were highly reproducible between the two valves from the same specimen ($R^2 = 0.84$, *p*-value < 0.001; Table 2). Reproducibility was also observed between HP and OSL ($R^2 = 0.35$, *p*-value < 0.001; Fig. 4; Table 2). While the OSL and HP signals showed obvious co-variations between 1981 and 2003 (i.e., 2003 is when peaks started to cover more than one year), the match was poor from 2004 to 2016. HP peaks in the 2004–2016 period became broader and the background level progressively increased until the ventral margin (i.e., maximum growth of the shell) while OSL peaks were still well defined with no change in the background level. Nevertheless, these two signals clearly follow the same overall trend (Fig. 4). Between 1981 and 2003, the reproducibility was higher than for the entire time period ($R^2 = 0.61$; $R^2 = 0.35$, respectively; Table 2); the coefficient was lower for the 2004–2016 period but still significant ($R^2 = 0.1$, *p*-value < 0.001; Table 2).

3.2. Ba/Ca_{shell} synchrony between HPs from different specimens

Ba/Ca_{shell} variations from the HP of 14 individuals are shown in Fig. 5. Only the first 10–25 years of life were analyzed for specimens older than 50 years unlike younger specimens, where the whole HP was analyzed. Shell records overlapped by 2–43 years, except for three periods of time where only one shell was analyzed (Fig. 6). Overall, the HP Ba/Ca_{shell} ratio of these 14 specimens ranged from 0.26 to 27.84 μmol mol^{-1}. Ba/Ca_{shell} variations of contemporaneous specimens were very similar in both the timing and magnitude of the peaks, as well as for the background levels. Pairwise correlations of annual maximum Ba/Ca_{shell} ratios for common growth periods were high, with a mean of 0.79 except for two coefficients where the correlations were negative (shells A140916 vs. A210916, shells A690916 vs. A050718; Fig. 6). When at least three common years of shell growth were compared, all correlation coefficients were positive and statistically significant (*p*-value < 0.01) when the common period was at least four years. Correlations between individuals <50-years-old (shell IDs A710916, A690916, and A060916, for which the whole HP was analyzed) were still significant, with a mean of 0.8 ± 0.03, even if the Ba/Ca_{shell} record was not clear for the last years of growth (2003–2016). A mean of all Ba/Ca_{shell} signals was calculated, showing that the average Ba/Ca_{shell} variations from 1893 to 2016 ranged from 0.388 to 24.52 μmol mol^{-1}.

3.3. Annually-resolved master chronology of Ba/Ca_{shell}

The synchrony of Ba/Ca_{shell} signals between samples allows us to propose an annually-resolved master chronology of Ba/Ca_{shell} from 1893 to 2016. The averages of all maximum Ba/Ca_{shell} for each year were calculated (range: 1.26–25.35 μmol mol^{-1}; Fig. 7). Given that the HP Ba/Ca_{shell} peaks of the three youngest individuals were poorly defined and broader between 2004 and 2016 (Fig. 5), the master chronology was created by clustering the Ba/Ca_{shell} ratios measured in HPs of the 14 specimens until 1980 and in the OSL of shell A710916 from 1981 onwards. Indeed, knowing that the maximum Ba/Ca_{shell} ratio per year from the HP of shell A710916 overlapped perfectly with the annually-resolved Ba/Ca_{shell} without A710916 and that, as indicated by linear regression, the annually-resolved Ba/Ca_{shell} and the maximum annual OSL Ba/Ca_{shell} were highly reproducible (Table 2), OSL Ba/Ca_{shell} values can replace HP values. EPS values were calculated only for HPs and showed values higher than the 0.85 threshold for most year, except for time periods with only one shell.

The Ba/Ca_{shell} master chronology tends to increase around 1980 onwards with a bump starting around 1925 to 1948 with higher values in 1933 and 1934. Despite these increases, the master chronology tends to remain in the range of 1.26–16.16 μmol mol^{-1} from 1893 to 1985. The increase period since 1977 shows two strong declines from 1999 to 2002 and in 2008.

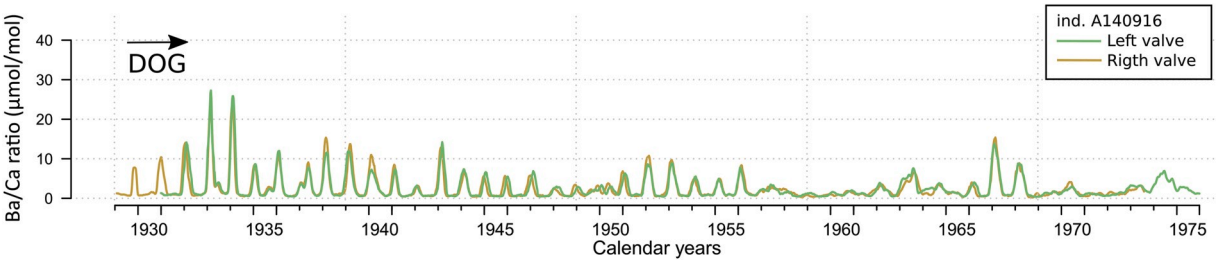

Fig. 3. Comparison of the Ba/Ca_{shell} ratio between the right valve (orange) and the left valve (green) from the same individual (shell ID A140916). DOG: Direction of Growth. (For interpretation of the references to colour in this figure legend, the reader is referred to the Web version of this article.)

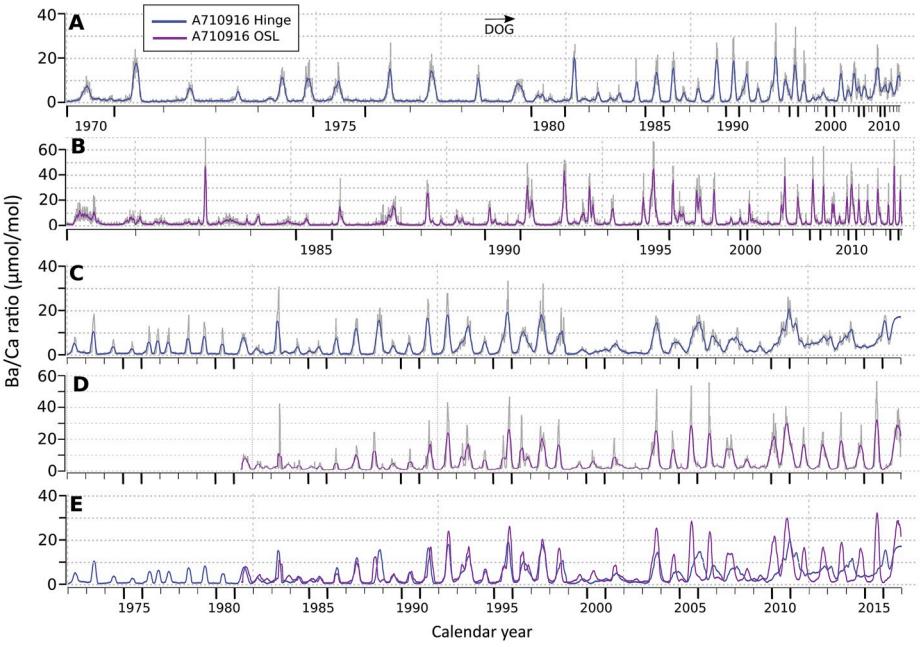

Fig. 4. Temporal variations of the Ba/Ca_{shell} ratio from HP and OSL from the same specimen (shell A710916). (A) 10-pt running mean (blue line) of the raw Ba/Ca_{shell} data (grey line) measured in HP. (B) 10-pt running mean (purple line) of the raw Ba/Ca_{shell} data (grey line) measured in OSL. (C, D) Same data presented after re-sampling with AnalySeries software to give the same weight to each annual increment. (E) Superposition of re-sampled Ba/Ca_{shell} ratios from HP and OSL, highlighting the offset between these time series from 2003 on. (For interpretation of the references to colour in this figure legend, the reader is referred to the Web version of this article.)

3.4. Biological and physical effects on the master chronology

3.4.1. Temporal dynamics of chlorophyll a concentration

To estimate the potential of Ba/Ca_{shell} ratio as a proxy for phytoplankton dynamics, we compared local and large-scale (see section 2.6 for details) concentrations of Chl *a* and Ba/Ca_{shell} in *A. islandica* specimens collected in SPM. Between 1998 and 2016 (common period for remote sensing data and shell records), the annually-resolved Ba/Ca_{shell} values were significantly correlated with the surface Chl *a* concentration. Correlation was positive ($r = 0.53$; $p = 0.02$) around SPM (local scale) for July (Fig. 8A). In the Northwestern Atlantic (large scale), correlations were positive in June and July close to SPM, in the South of Newfoundland (region 1) and in the central Labrador Sea (region 3). Interestingly, the magnitude of Ba/Ca_{shell} peaks was positively correlated in May and negatively correlated in June with Chl *a* concentration in the cold waters along the Labrador and Newfoundland shelf (region 2), and along the southwest coast of Greenland (region 4) (Fig. 8B).

3.4.2. Climate variations

Ocean oscillation indices were compared to the annually-resolved Ba/Ca_{shell} master chronology and correlation coefficients were calculated. A statistically significant negative correlation was found with NAO (1893–2016: $r = -0.24$, $p < 0.01$; 1998–2016: $r = -0.54$, $p = 0.016$) while our master chronology was significantly and positively correlated with AMO (1893–2016: $r = 0.44$, $p < 0.001$; 1998–2016: $r = 0.52$, $p = 0.024$). When AMO was in positive phases and NAO in negative one, the magnitudes of the Ba/Ca_{shell} peaks were higher.

4. Discussion

4.1. Methodological aspect

4.1.1. Assessment of the intra-shell reproducibility of Ba/Ca_{shell} signal

Over the past decade, barium incorporation into bivalve shells has been the subject of numerous studies, especially on short-lived bivalves such as scallops (*Comptopallium radula*; Thébault et al., 2009, *Pecten maximus*; Gillikin et al., 2008), clams (*Saxidomus gigantea;* Gillikin et al., 2008, *Ruditapes philippinarum*; Poulain et al., 2015), or on juvenile specimens of long-lived species such as *Tridacna gigas* (Elliot et al., 2009) and *Arctica islandica* (Schöne et al., 2013), and more recently on ontogenetically old long-lived *A. islandica* (Marali and al., 2017b). However, only a few studies compared the Ba/Ca_{shell} signal from the same specimen to test for the intra-individual variability (Elliot et al., 2009). Elliot et al. (2009) analyzed the OSL, the inner shell layer and the HP of the giant long-lived *Tridacna gigas* and found similar signals, although analyses were performed only on young specimens (17–22 years old). More recently, Marali et al. (2017a) demonstrated the high reproducibility of HP signals by re-analyzing the HP of an old *A. islandica* specimen after re-polishing of the shell surface that had previously been laser ablated. In our study, we highlight the reproducibility of Ba/Ca_{shell} between two structures of a same specimen. Geochemical records in the HP, whether cut from the left or the right valve, were highly reproducible within a specimen. We found the same result when comparing Ba/Ca signals from the OSL and HP of a same individual. These findings suggest a similar time period of calcification of the right and left valves for the HP and OSL with the same mechanism. Indeed, the OSL and the HP are biomineralized at the same site of shell formation (i.e., fluid-filled outer extrapallial space) by the outer extrapallial fluid (Crenshaw, 1980; Schöne and Surge, 2012). Reproducibility of Ba/Ca_{shell} between OSL and HP highlights the lack of relationship between shell growth rate and the Ba/Ca record: even though the OSL grows much faster than the HP, the Ba/Ca_{shell} peak magnitudes are equivalent. The lack of a significant difference in the geochemical signals archived in the left and right parts is crucial because it indicates that empty single valves collected on the seafloor can be incorporated into a master chronology without any bias. This offers the opportunity to extend such a geochemical record even further into the past without worrying about the chirality of the valve. Selecting the OSL or the HP for geochemical analyses does not influence the final record: both parts incorporate barium in a similar way. Thus the decision to choose any part of the shell need only be based on technical or economic considerations.

4.1.2. Potential reasons for a decrease in synchrony with age

Sclerochronological investigations usually seek shell parts that provide the most complete and precise (i.e., high resolution) record. The use of the HP generally ensure perfect preservation of the record (e.g. limited attacks by euendoliths, reduced bioerosion and virtually no chance of breakage) and reduces work time and analytical costs. Because of its size (e.g. six times smaller than the OSL in *A. islandica* specimens from SPM), the temporal resolution of the geochemical record is lower

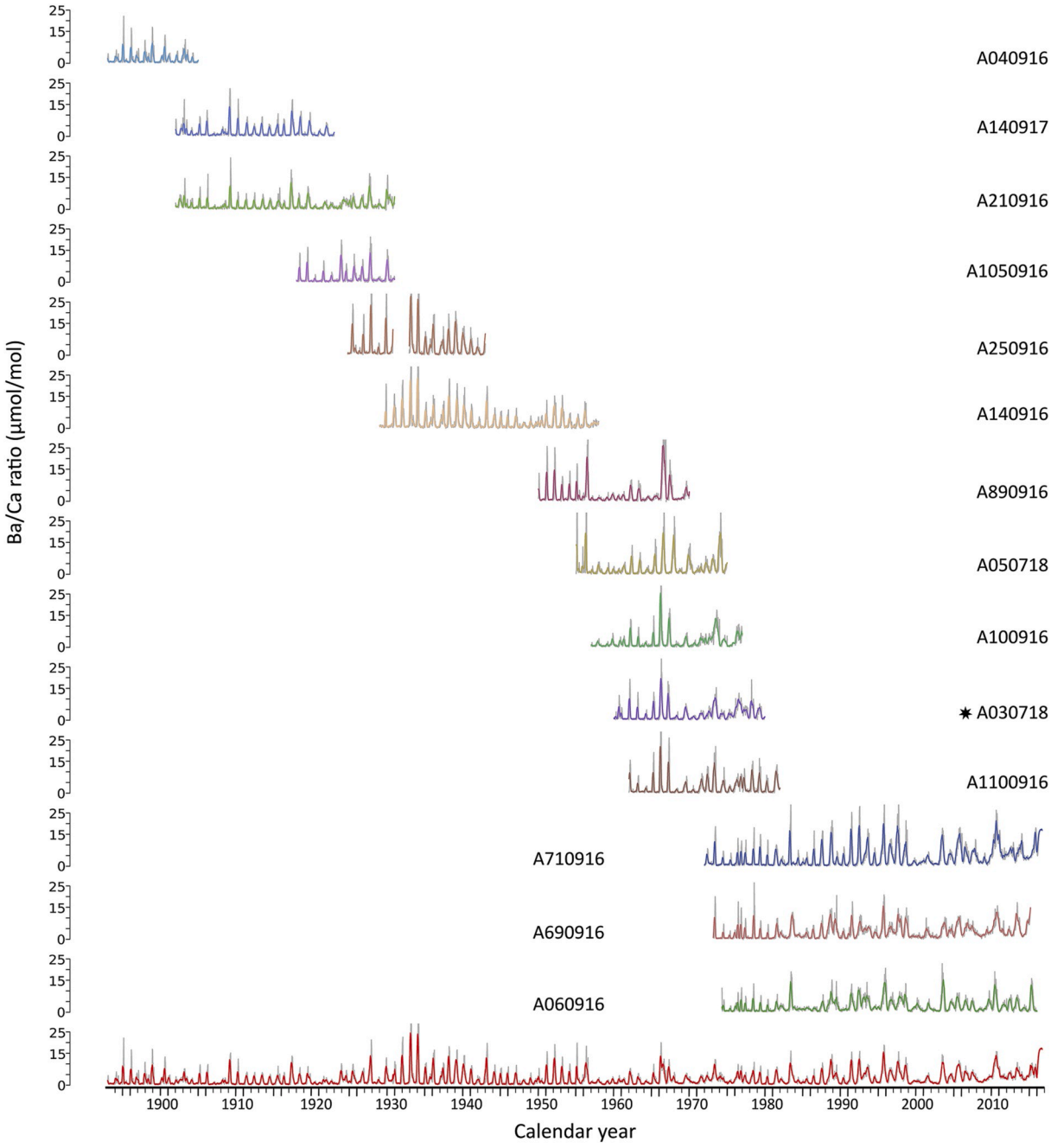

Fig. 5. Ba/Ca_{shell} records in HPs of 14 individuals, arranged according to their hatch year. The bottom red curve represents the mean of all 14 specimens. For each individual, re-sampled data (50 measurements per year) are represented by the grey line while the 10-pt running mean is displayed in colour. The specimen marked with a black asterisk was already dead when collected (shell ID A030718). (For interpretation of the references to colour in this figure legend, the reader is referred to the Web version of this article.)

than in the OSL. A flat background and sharp peaks are common Ba/Ca_{shell} features in the HP and OSL. However, LA-ICP-MS analyses in our shells carried out in the HP resulted in lower Ba/Ca_{shell} ratios and less well-defined peaks in comparison with the OSL because of time averaging. This phenomenon leads to a decrease in reproducibility between HP and OSL that results from the progressive signal separation over time (Fig. 4; Table 2). Elliot et al. (2009) showed no such difference between HP, OSL, and inner shell layer, probably because they worked on a giant species that reaches 1.5 m in length with a lifespan of 100 years. The annual width increments of the giant clams are therefore not comparable with those in *A. islandica*, which has a substantially slower growth rate. Ba/Ca_{shell} peaks in *A. islandica* HP would very likely be similar in magnitude to those in the OSL if the measurements were not slightly averaged due to the laser spot size and the growth rate difference between HP (in which time is condensed) and OSL (Fig. 4).

Likewise, Ba/Ca_{shell} peaks from slower growing (old) parts become broader and the background level tends to increase, especially with ontogenetically old specimens. Gillikin et al. (2006) attributed these fluctuations of Ba/Ca_{shell} background levels in *Mytilus edulis* to salinity. However, their study was performed in estuaries where salinity fluctuations are high compared to our study site where freshwater inputs are limited and salinity remains almost constant (31.42 ± 0.03; Poitevin et al., 2018). More recently, Marali et al. (2017a), working on old *A. islandica* specimens, rejected the hypothesis of a physiological aging

Table 2
Results of Pearson's product-moment correlation (r) and linear regression analysis. Each result came from the comparison between parts of a specimen where a 10-pt running mean was applied. A coefficient of determination (R^2) and the associated *p*-value were calculated for different time periods.

Sample comparison	Years	r	R^2	*p*-value
A140916_LV vs A140916_RV	all	0.92	0.84	<0.001
A710916_HP vs A710916_OSL	all	0.59	0.35	<0.001
	1981–2003	0.78	0.61	<0.001
	2004–2016	0.33	0.1	<0.001
Annually-resolved:	1981–2016	0.83	0.67	<0.001
Ba/Ca_{shell} vs A710916_OSL	1981–2003	0.87	0.75	<0.001
	2004–2016	0.9	0.79	<0.001

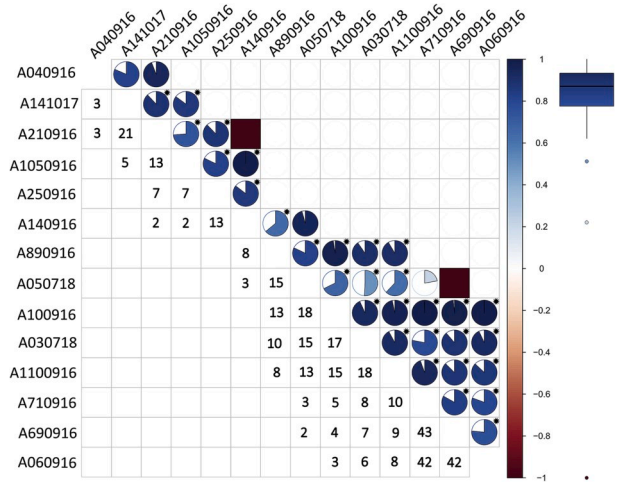

Fig. 6. Pairwise correlation matrix between annual maximum Ba/Ca_{shell} ratios for common growth periods of the 14 individuals, and boxplot of correlation coefficients. The upper triangle represents correlations by pie charts in a positive correlation case and square for a negative one, and the lower triangle displays the duration of the common growth period (in years) used to calculate the correlation coefficient. Percentage of fill and colour indicate the strength of correlation (e.g., full square of dark red for a negative correlation −1 and full circle of dark blue for a positive correlation +1). Correlations marked with black asterisks have significant *p*-values (α = 1%). (For interpretation of the references to colour in this figure legend, the reader is referred to the Web version of this article.)

effect on background Ba/Ca_{shell}. They suggested that the sampling resolution was not sufficient to separate peaks from background when increments become smaller than the laser spot size (signal smearing) due to time averaging. Our results agree with their findings. We propose that limited time averaging can only be achieved by selecting the best balance between the width of annual increments (because wide increments provide better temporal resolution) and the diameter of the laser beam (large beams lower the detection limits of the ICP-MS whereas small ones increase the temporal resolution). Ways to avoid signal smearing are then (i) to reduce the spot size as the laser moves towards ontogenetically older parts and/or (ii) to analyze only the first years of life of old specimens. Here, we chose the latter solution and so selected specimens with overlapping lifespan and only analyzed the first decades of HP growth to focus on annual increments far wider than the laser spot diameter. This strategy allowed us to generate a continuous, 124-year-long chronology of high-resolution Ba/Ca_{shell} ratio.

4.1.3. *Profile of Ba/Ca_{shell} as a new cross-dating tool*

Cross-dating techniques come from dendrochronology and are applied to shell growth increment width data. Cross-dating ensures that each annual increment is assigned its exact year of calcification through a comparison of narrow and wide increments patterns among shells from the same population. It is then useful to correct errors arising from missed or falsely identified increments (Douglass, 1941; Stokes and Smiley, 1968; Wigley et al., 1987). However, in bivalve sclerochronology, cross-dating is still a challenge. The EPS threshold is difficult to reach with a limited sample depth. Construction of a robust, annually-resolved master chronology requires "ideal" samples with clearly developed annual growth patterns and an experienced reader. Because of high inter-individual synchrony and the reproducibility of annually-resolved Ba/Ca_{shell} time series demonstrated in this study, we strengthen the concept proposed by Marali et al. (2017b) to use Ba/Ca_{shell} as a new cross-dating tool. Indeed, annual Ba/Ca_{shell} time-series can be used (i) to cross-validate the result of cross-dating based on increment width, (ii) to check whether lifespans of different specimens overlap, and (iii) to determine if a dead-collected specimen matches an existing master chronology and therefore identify its dates of hatch and death.

A statistically robust master chronology built on shell growth increment width generally requires many "ideal" specimens. The SGI master chronology built by Poitevin et al. (2019), whose shells were used in this paper, needed at least seven shells to reach the EPS threshold of 0.85. Occasionally, the minimum required sample depth has been found to be four shells (Estrella-Martínez et al., 2019). In our study,

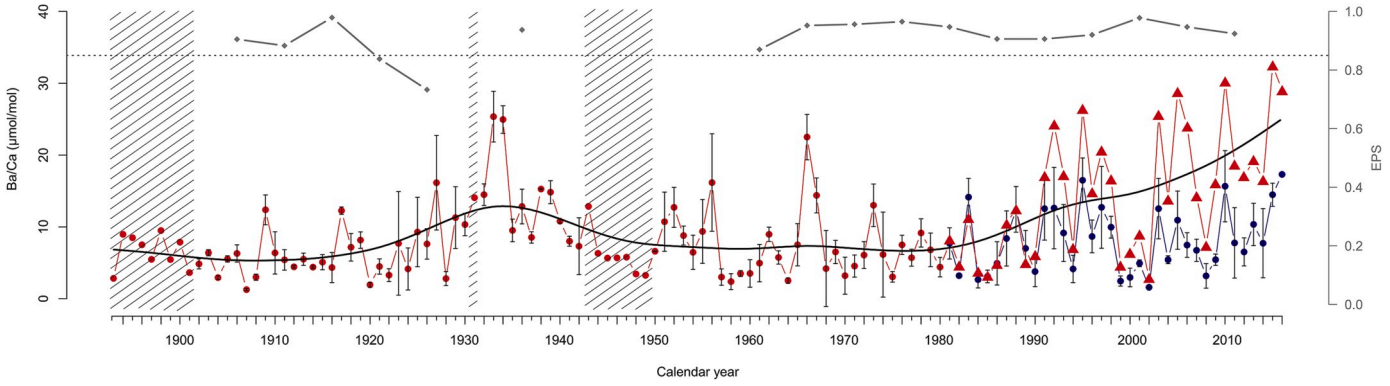

Fig. 7. Annually-resolved Ba/Ca_{shell} master chronology in red built with HP data until 1980 (filled red circles) and with OSL data from 1981 onwards (filled red triangles). Annually-resolved Ba/Ca from HP only (filled circles) are shown in red from 1893 to 1980 and in blue starting from 1981. Standard deviations are represented by vertical black lines. Striped zones represent the three periods with only one HP. EPS values for HP data are displayed in grey diamond connected by solid lines; the dotted line shows the 0.85 threshold. EPS values were calculated using eight-year window and three-year window overlaps. Trend (smooth spline with 10 degrees of freedom) of the annually-resolved Ba/Ca_{shell} master chronology is indicated by a solid black line from 1893 to 2016. (For interpretation of the references to colour in this figure legend, the reader is referred to the Web version of this article.)

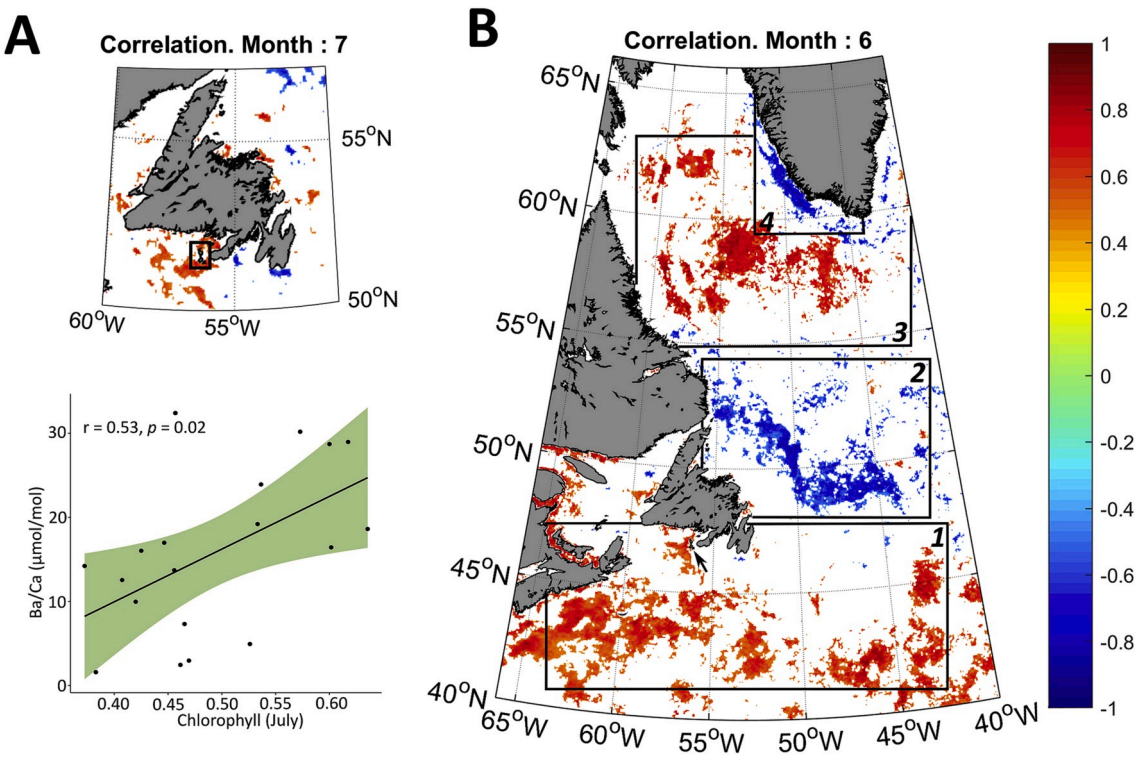

Fig. 8. Correlation between the annually-resolved Ba/Ca_{shell} master chronology (i.e., OSL of shell A710916) and the average chlorophyll *a* concentration in June and July. (A) Zoom in on the spatial correlation map for July and correlation between monthly mean of surface chlorophyll and the master Ba/Ca_{shell} master chronology around SPM (local scale indicated by the black square) in July (common period: 1998–2016). (B) Spatial correlation maps in June (area: 40–66°N/40–60°W; period: 1998–2016). Only statistically significant correlations (α = 5%) are represented. White areas indicate either a lack of chlorophyll *a* data or non-significant correlations. The black arrow points towards the SPM archipelago (close to the sample site). Delimited regions are south of Newfoundland (region 1), northeastern of Newfoundland (region 2), center of the Labrador Sea (region 3) and southwestern of Greenland (region 4).

sufficient statistics were provided with only two shells. In concrete terms, we highlight the relevance of barium-based cross-dating to improve EPS values with only a few specimens and therefore a drastically decreased sampling effort.

4.2. *Environmental control on Ba/Ca$_{shell}$*

The high inter-individual reproducibility of Ba/Ca_{shell} profiles strongly indicates the existence of an environmental driver controlling the incorporation of barium in shells. In the case of coastal water bivalves, two factors have been proposed: (i) the input of terrigenous Ba coming from riverine and freshwater inputs and (ii) the input of biogenic Ba coming from phytoplankton blooms.

4.2.1. *Potential influence of the St. Lawrence River*

Our study site is located 6 km away from the mouth of Belle-Rivière, the main river of SPM. We cannot exclude that this small watershed (i.e., length of the river corridor = 13 km; watershed surface <500 km^2) transports terrestrial material, including terrigenous barium, to the SPM coastal zone. However, because the size of the watershed is small and the geology mainly consists of volcanic and sedimentary rocks, the release of barium from chemical and/or mechanical weathering is probably weak and constant at the scale of *A. islandica* lifespans. In addition, the role of the St. Lawrence River, one of the biggest rivers in North America and located several hundred of kilometers away at Quebec City has also been explored. Poitevin et al. (2019) reported the lack of a significant correlation between shell growth rate and the St. Lawrence River inflows. Here, we tested this relationship on the Ba/Ca_{shell} master chronology and also found no significant correlation. Freshwater discharge from the St. Lawrence plays a dominant role in driving circulation over the northwestern Gulf of St. Lawrence (Sheng, 2001). Near the mouth of the St. Lawrence estuary, upstream inflow and upwelling water from the northwestern Gulf generate a jet-like feature known as the Gaspé Current (Fig. 1A). The Gaspé Current is a buoyancy-driven coastal jet that flows seaward along the coast of Gaspé Peninsula, moving warmer and brackish water to the Baie des Chaleurs and then to the southeastern Gulf, with a lag a several months. This current never reaches the SPM archipelago (Galbraith et al., 2017).

4.2.2. *Relationship with phytoplankton dynamics*

Previous studies associated shell Ba concentration with Ba-rich phytoplankton (mostly diatom species); these phytoplankton can be directly ingested by filter-feeding bivalves (Stecher et al., 1996). Alternatively, barium, under the form of barite crystals ($BaSO_4$) after its reaction with SO_4, can be passively incorporated. The establishment of anoxic conditions in decaying diatom aggregates promotes this reaction (Vander Putten et al., 2000; Lazareth et al., 2003). To our knowledge, there are no available data on the growth period of *A. islandica* or other bivalve shells in SPM. The closest location with relevant data lies south of the Gulf of Maine, on the Nantucket Shoals, where Weidman et al. (1994) reported that *A. islandica* produces shell monitoring the environment from May to December. Given (i) that seawater temperature variations are very similar on the Nantuckets Shoals and in SPM (Weidman et al., 1994; Poitevin et al., 2018), and (ii) that Ba/Ca_{shell} maxima occur in the first third or first half of annual growth increments (Fig. 4), Ba/Ca_{shell} peaks are likely produced in early summer (around June–July). Therefore, we compared Chl *a* data obtained by remote sensing for June and July with our annually-resolved Ba/Ca_{shell} master chronology. Our goal was to compare variations in surface Chl *a* data with Ba/Ca incorporated into *A. islandica* shells at a local scale (i.e.,

around SPM) and then at a much large scale (i.e., the Northwestern Atlantic) (see section 2.6 for details). A positive correlation was found at the local scale for the month of July ($r = 0.53$; $p = 0.02$; Fig. 8A). It would be surprising to obtain a higher correlation coefficient since Chl *a* data come from satellite sensors that derive Chl *a* from ocean surface colour. Surface Chl *a* data are only a subset of the actual Chl *a* concentration in the water column where the Deep Chlorophyll Maximum is deeper and may vary as a function of light and nutrient availability (Mignot et al., 2014). In addition, remote sensing data do not provide information on the taxonomic composition of phytoplankton communities. Requirements for barite crystal formation are likely not met during a dinoflagellate bloom. No significant correlation was found for June ($r = 0.35$, $p = 0.14$).

At a larger scale, significant correlations were found with surface Chl *a* concentration in June and July not only around SPM but also in some parts of the Northwestern Atlantic Ocean (Fig. 8B). Here, we chose to focus our reflection on the correlation map in June due to stronger and detailed patterns. Positive and negative correlations indicate that surface Chl *a* concentration fluctuates in the same way as the master Ba/Ca_{shell} chronology measured in *A. islandica* (i.e., variations of maximum Ba/Ca per year) and in the opposite way, respectively. We must, however, keep in mind that a significant correlation does not imply a direct relationship (antagonistic or not), especially when the correlation is far away from SPM. It is unlikely that a phytoplankton bloom in the central Labrador Sea can be directly responsible for a Ba peak in shells at SPM. Because the inshore and offshore branches of the Labrador Current have a surface velocity of 0.2 and 0.4 m s^{-1}, respectively (Han et al., 2008) implying a transfer time of several months between the central Labrador Sea and SPM, excluding a direct relationship. Nevertheless, our results demonstrate a strong link between the master Ba/Ca_{shell} chronology and the early summer chlorophyll *a* concentration in the Northwestern Atlantic, at least over the last 2 decades (1998 and 2016; Fig. 8). Depending on geographic location, however, correlations are opposite. In the south of Newfoundland shelf (region 1) and in the center of the Labrador Sea (region 3), correlations are positive and they are negative in the Southwestern Greenland (region 4) and in the Northeastern Newfoundland shelf (region 2) (Fig. 8B).

The phenology of the phytoplankton spring bloom probably explains this pattern. Lacour et al. (2015) used a cluster k-means analysis to assemble pixels exhibiting similar seasonal variations of Chl *a* and obtained by bioregionalization of the North Atlantic Ocean, 6 different regions so-called "bioregions". Three of these bioregions seem to coincide with our 4 regions. Indeed, the spring bloom onset in regions 2 and 4, gathered in one bioregion, occurs approximately at the same time in May-early June (Afanasyev et al., 2001; Nezlin et al., 2002; Wu et al., 2008; Frajka-Williams and Rhines, 2010; Marchese et al., 2019) and is triggered by a salinity stratification (Wu et al., 2008; Lacour et al., 2015; Hetzinger et al., 2013). In region 3 (i.e., center of the Labrador Sea), onset of the bloom occurs with a delay of 1 month (i.e., in June) (Frajka-Williams and Rhines, 2010) and is linked to cooling-to-heating shift in air-sea heat fluxes (Marchese et al., 2019). For the region 1 including SPM, spring bloom is triggered by thermal stratification (Zhai et al., 2011) and occurs in April (Afanasyev et al., 2001; Nezlin et al., 2002; Zhai et al., 2011). In view of our spatial correlations, one would expect that positive correlations are linked to the amplitude of the spring bloom. Indeed, during any spring blooms in the Northwestern Atlantic Ocean, the master Ba/Ca_{shell} chronology is positively correlated to the surface Chl *a* concentration. These results demonstrate an overall influence of physical factors on the phenology of spring blooms in the Northwestern Atlantic. Positive correlations in region 1 and 3 after their spring bloom period (i.e., June to September for the region 3 and May to July for region 1), suggest that drivers can also influence regions post-spring bloom, meaning that conditions (i.e., nutrients, light, temperature) are still favorable. Zhai et al. (2011) described the phenology of the spring bloom in the Scotian Shelf and Slope and deep ocean near the Gulf Stream (i.e., region 1) and highlighted a constant replenishment of nutrients via upwelling in some parts of the studied area. In addition, region 3 is not limited by nutrients leading to a persistent biomass all summer long (Lacour et al., 2015). However, in regions 2 and 4, the correlation shifts from positive in May (i.e., timing of the spring bloom) to negative in June. This pattern might be explained by the nutrient-limitation in these regions. In the regions 4 (Southeastern of Greenland coast) and 2 (Northeastern of the Newfoundland Shelf) rapid bloom decline can be caused by nitrate depletion (Lacour et al., 2015, Harrison and Li, 2008; Harrison et al., 2013) and/or light-limitation by self-shading for region 4 only (Marra, 2004).

Poitevin et al. (2019) suggested that concentration of Chl *a* at Saint-Pierre and Miquelon (SPM) is influenced by the Labrador Current. This current may bring nutrients to the oligotrophic SPM environment to trigger bloom when conditions of light and temperature are favorable. Nevertheless, Chl *a* is decreasing drastically in early-June upstream of SPM (i.e., in region 2) (Afanasyev et al., 2001), sign of a depletion in nutrients in the Labrador Current thereafter. Based on the speed transport in Han et al. (2008), Labrador Current water around 53°N takes around 2 months to attain SPM. Thus, nutrients-poor Labrador Current water will reach SPM area around August leaving June and July with inflow of nutrients-rich water.

4.2.3. Insights into Northwestern Atlantic climate variability

Our study highlights a potential relationship between variations of Ba/Ca_{shell} and physical drivers influencing amplitude, timing and duration of phytoplankton blooms in the Northwestern Atlantic Ocean. Indeed, these characteristics are dependent upon physical forcing of the ocean (e.g. light level, temperature, ice, stratification, mixed layer depth and nutrients supply) that are directly modified by climatological drivers (e.g. cloud cover, solar radiation, wind stress and upwelling) (Behrenfeld and Boss, 2014). Climate-ocean drivers are reported to be linked to the productivity by modifying physical processes of blooms (Chiba et al., 2012; Racault et al., 2012). In the North Atlantic Ocean, the Atlantic Multidecadal Oscillation (AMO) and North Atlantic Oscillation (NAO) correlated to the Atlantic Meridional Overturning Circulation (AMOC) are the atmospherics and oceanic, respectively, large-scale modes influencing the phenology of phytoplankton blooms (Henson et al., 2009; Drinkwater et al., 2013; Harrison et al., 2013). Our study shows an increasing trend of the Ba/Ca ratio around 1970 to 2016 which may result from an increase in productivity. Ba/Ca_{shell} in SPM was correlated positively with the AMO (1893–2016: $r = 0.44$, $p < 0.001$; 1998–2016: $r = 0.52$, $p = 0.024$) and negatively with the NAO (1893–2016: $r = -0.24$, $p < 0.01$; 1998–2016: $r = -0.54$, $p = 0.016$). These observations highlight a link with warm phases of the climate-ocean state. Indeed, results from Sherwood et al. (2011) indicated a persistence of warm and nutrient-rich regime since the 1970s in the Western North Atlantic. Ocean warming and input of freshwater from Arctic ice melting should play a significant role in the phenology of the bloom. As reported the Fifth Assessment Report of the Intergovernmental Panel on Climate Change, the strength of the AMOC is weakening (Collins et al., 2013) leading to a cooling in the subpolar Atlantic Ocean and a warming in the Gulf Stream region (Caesar et al., 2018). The AMOC is also influenced by ice melting (Yu et al., 2016) and an enhancement of primary production is observed in Northern regions (Drinkwater et al., 2014).

5. Conclusions

The Ba/Ca shell master chronology built in our study (Fig. 7) is in agreement with the increase of phytoplankton production over the last 2 decades. The synchrony between the summer production in the SPM region, Northwestern Atlantic ocean, and the Ba/Ca record in coastal bivalves is still not clear and needs further investigations. Nevertheless, the use of Ba/Ca record and growth rate of *A. islandica* (Poitevin et al., 2019) with spatial statistical analysis appears as a powerful set of tools to monitor the phytoplankton dynamics at regional and, probably, at

global scales. Thus, further studies are required to get a mechanistic understanding of the incorporation of Ba in shells of marine bivalves, in presence of different types of blooms and how decadal oscillations in primary production influence Ba/Ca_{shell}.

Declaration of competing interest

The authors declare that they have no known competing financial interests or personal relationships that could have appeared to influence the work reported in this paper.

CRediT authorship contribution statement

Justine Doré: Methodology, Writing - original draft, Visualization, Conceptualization. **Gwénaëlle Chaillou:** Conceptualization, Writing - review & editing. **Pierre Poitevin:** Methodology, Writing - review & editing. **Pascal Lazure:** Methodology. **André Poirier:** Methodology. **Laurent Chauvaud:** Conceptualization, Writing - review & editing. **Philippe Archambault:** Conceptualization, Writing - review & editing. **Julien Thébault:** Conceptualization, Writing - review & editing.

Acknowledgements

This research is a contribution of LIA-BeBEST, an international collaboration between French (IUEM-UBO, LEMAR - Brest) and Canadian (ISMER-UQAR, Rimouski) academic institutions. We thank the LEMAR and the DFO for their help. We are sincerely grateful to Dr. Virginie Roy (MLI, Québec-Canada) for her relevant advice and her kindness. In addition, we express our sincere gratitude to Dr. Simon Bélanger (UQAR) and Dr. Peter Galbraith (MLI) for their help to disentangle the information and Herlé Goraguer (Ifremer delegate in SPM) for his commitment to the preparation and sending of a part of the samples. We show our appreciation to Laure Devine and Hannah Whitby for their useful comments. We also thank Eric Dabas for his technical assistance in the sclerochronology process. Finally, we would like to thank the two anonymous reviewers for their valuable comments and suggestions in a previous version of the manuscript. This research was supported by a grant from the Natural Sciences and Engineering Research Council of Canada (to G.C.) and the Canada Research Chair Program (to G.C.) as well as the Région Bretagne and the Cluster of Excellence LabexMER. This research was carried out as part of the Ph.D. thesis of Justine Doré for the University of Western Brittany. All the data used to produce the results of this paper may be obtained by contacting the corresponding author.

Appendix A. Supplementary data

Supplementary data to this article can be found online at https://doi.org/10.1016/j.ecss.2020.106628.

References

Han, G., Tang, C.L., 2001. Interannual variations of volume transport in the western Labrador Sea based on TOPEX/poseidon and WOCE data. J. Phys. Oceanogr. 31, 199–211. https://doi.org/10.1175/1520-0485(2001)031<0199:IVOVTI>2.0.CO;2.

Purton, L.M., Shields, G.A., Brasier, M.D., Grime, G.W., 1999. Metabolism controls Sr/Ca ratios in fossil aragonitic mollusks. Geology 27, 1083–1086. https://doi.org/10.1130/0091-7613(1999)027<1083:MCSCRI>2.3.CO;2.

Afanasyev, Y.D., Nezlin, N.P., Kostianoy, A.G., 2001. Patterns of seasonal dynamics of remotely sensed chlorophyll and physical environment in the Newfoundland region. Remote Sens. Environ. 76, 268–282. https://doi.org/10.1016/S0034-4257(00)00209-1.

Ballesta-Artero, I., Janssen, R., van der Meer, J., Witbaard, R., 2018. Interactive effects of temperature and food availability on the growth of *Arctica islandica* (Bivalvia) juveniles. Mar. Environ. Res. 133, 67–77. https://doi.org/10.1016/j.marenvres.2017.12.004.

Behrenfeld, M.J., Boss, E.S., 2014. Resurrecting the ecological underpinnings of ocean plankton blooms. Ann. Rev. Mar. Sci. 6, 167–194. https://doi.org/10.1146/annurev-marine-052913-021325.

Bishop, J.K.B., 1988. The barite-opal-organic carbon association in oceanic particulate matter. Nature 332, 341–343. https://doi.org/10.1038/332341a0.

Bonitz, F.G.W., Andersson, C., Trofimova, T., Hátún, H., 2018. Links between phytoplankton dynamics and shell growth of *Arctica islandica* on the Faroe Shelf. J. Mar. Syst. 179, 72–87. https://doi.org/10.1016/j.jmarsys.2017.11.005.

Boyce, D.G., Lewis, M.R., Worm, B., 2010. Global phytoplankton decline over the past century. Nature 466, 591–596. https://doi.org/10.1038/nature09268.

Butler, P.G., Wanamaker, A.D., Scourse, J.D., Richardson, C.A., Reynolds, D.J., 2013. Variability of marine climate on the North Icelandic Shelf in a 1357-year proxy archive based on growth increments in the bivalve *Arctica islandica*. Palaeogeogr. Palaeoclimatol. Palaeoecol. 373, 141–151. https://doi.org/10.1016/j.palaeo.2012.01.016.

Caesar, L., Rahmstorf, S., Robinson, A., Feulner, G., Saba, V., 2018. Observed fingerprint of a weakening Atlantic Ocean overturning circulation. Nature 556, 191–196. https://doi.org/10.1038/s41586-018-0006-5.

Carré, M., Bentaleb, I., Bruguier, O., Ordinola, E., Barrett, N.T., Fontugne, M., 2006. Calcification rate influence on trace element concentrations in aragonitic bivalve shells: evidences and mechanisms. Geochem. Cosmochim. Acta 70 (19), 4906–4920. https://doi.org/10.1016/j.gca.2006.07.019.

Chiba, S., Batten, S., Sasaoka, K., Sasai, Y., Sugisaki, H., 2012. Influence of the pacific decadal oscillation on phytoplankton phenology and community structure in the Western North pacific. Geophys. Res. Lett. 39 https://doi.org/10.1029/2012GL052912.

Chmura, G.L., Santos, A., Pospelova, V., Spasojevic, Z., Lam, R., Latimer, J.S., 2004. Response of three paleo-primary production proxy measures to development of an urban estuary. Sci. Total Environ. 320, 225–243. https://doi.org/10.1016/j.scitotenv.2003.08.003.

Collins, M., Knutti, R., Arblaster, J., Dufresne, J.-L., Fichefet, T., Friedlingstein, P., Gao, X., Gutowski, W.J., Johns, T., Krinner, G., Shongwe, M., Tebaldi, C., Weaver, A. J., Wehner, M., 2013. Long-term Climate Change: Projections, Commitments and Irreversibility. Clim. Chang. 2013 Phys. Sci. Basis. Contrib. Work. Gr. I to Fifth Assess. Rep. Intergov. Panel Clim. Chang. Stocker (T.F., D. Qin, G.-K. Plattner, M. Tignor, S.K. Allen, J. Boschung, A. Nauels, Y. Xia).

Crenshaw, M.A., 1980. Mechanisms of shell formation and dissolution. Skelet. Growth Aquat. Org. Biol. Rec. Environ. 115–132. https://doi.org/10.1007/978-1-4899-4995-0_4. Chang. by Donald C. Rhoads Richard A. Lutz.

Dehairs, F., Chesselet, R., Jedwab, J., 1980. Discrete suspended particles of barite and the barium cycle in the open ocean. Earth Planet Sci. Lett. 49, 528–550. https://doi.org/10.1016/0012-821X(80)90094-1.

Douglass, A.E., 1941. Crossdating in dendrochronology. J. For. 39, 825–831. https://doi.org/10.1093/jof/39.10.825.

Drinkwater, K., Colbourne, E., Loeng, H., Sundby, S., Kristiansen, T., 2013. Comparison of the atmospheric forcing and oceanographic responses between the Labrador Sea and the Norwegian and Barents seas. Prog. Oceanogr. 114, 11–25. https://doi.org/10.1016/j.pocean.2013.03.007.

Drinkwater, K.F., Miles, M., Medhaug, I., Otterå, O.H., Kristiansen, T., Sundby, S., Gao, Y., 2014. The Atlantic Multidecadal Oscillation: its manifestations and impacts with special emphasis on the Atlantic region north of 60°N. J. Mar. Syst. 133, 117–130. https://doi.org/10.1016/j.jmarsys.2013.11.001.

Dymond, J., Suess, E., Lyle, M., 1992. Barium in deep-sea sediment: a geochemical proxy for paleoproductivity. Paleoceanography 7, 163–181. https://doi.org/10.1029/92PA00181.

Elliot, M., Welsh, K., Chilcott, C., McCulloch, M., Chappell, J., Ayling, B., 2009. Profiles of trace elements and stable isotopes derived from giant long-lived *Tridacna gigas* bivalves: potential applications in paleoclimate studies. Palaeogeogr. Palaeoclimatol. Palaeoecol. 280, 132–142. https://doi.org/10.1016/j.palaeo.2009.06.007.

Emberton, S., Chittka, L., Cavallaro, A., Wang, M., 2015. Sensor capability and atmospheric correction in ocean colour remote sensing. Rem. Sens. 8, 1. https://doi.org/10.3390/rs8010001.

Estrella-Martínez, J., Ascough, P.L., Schöne, B.R., Scourse, J.D., Butler, P.G., 2019. 8.2 ka event North Sea hydrography determined by bivalve shell stable isotope geochemistry. Sci. Rep. 9, 6753. https://doi.org/10.1038/s41598-019-43219-1.

European Environment Agency, 2005. The European Environment: State and Outlook 2005. European Communities.

Feng, J.F., Zhu, L., 2012. Changing trends and relationship between global ocean chlorophyll and sea surface temperature. Procedia Environ. Sci. 13, 626–631. https://doi.org/10.1016/j.proenv.2012.01.054.

Frajka-Williams, E., Rhines, P.B., 2010. Physical controls and interannual variability of the Labrador Sea spring phytoplankton bloom in distinct regions. Deep-Sea Res. Part I Oceanogr. Res. Pap. 57, 541–552. https://doi.org/10.1016/j.dsr.2010.01.003.

Galbraith, P.S., Chassé, J., Gilbert, D., Larouche, P., Brickman, D., Pettigrew, B., Devine, L., Gosselin, A., Pettipas, R.G., Lafleur, C., 2017. Physical Oceanographic Conditions in the Gulf of St. Lawrence in 2016. Canadian Science Advisory Secretariat.

Genovesi, L., de Vernal, A., Thibodeau, B., Hillaire-Marcel, C., Mucci, A., Gilbert, D., 2011. Recent changes in bottom water oxygenation and temperature in the Gulf of St. Lawrence: micropaleontological and geochemical evidence. Limnol. Oceanogr. 56, 1319–1329. https://doi.org/10.4319/lo.2011.56.4.1319.

Gillikin, D.P., Lorrain, A., Navez, J., Taylor, J.W., André, L., Keppens, E., Baeyens, W., Dehairs, F., 2005. Strong biological controls on Sr/Ca ratios in aragonitic marine bivalve shells. Geochem. Geophys. Geosyst. 6, 5. https://doi.org/10.1029/2004GC000874.

Gillikin, D.P., Dehairs, F., Lorrain, A., Steenmans, D., Baeyens, W., André, L., 2006. Barium uptake into the shells of the common mussel (*Mytilus edulis*) and the potential for estuarine paleo-chemistry reconstruction. Geochem. Cosmochim. Acta 70, 395–407. https://doi.org/10.1016/j.gca.2005.09.015.

Gillikin, D.P., Lorrain, A., Paulet, Y.-M., André, L., Dehairs, F., 2008. Synchronous barium peaks in high-resolution profiles of calcite and aragonite marine bivalve shells. Geo Mar. Lett. 28, 351–358. https://doi.org/10.1007/s00367-008-0111-9.
Gregg, W.W., 2005. Recent trends in global ocean chlorophyll. Geophys. Res. Lett. 32, L03606 https://doi.org/10.1029/2004GL021808.
Häkkinen, S., Rhines, P.B., 2004. Decline of subpolar North Atlantic circulation during the 1990s. Science 304, 555–559. https://doi.org/10.1126/science.1094917.
Han, G., 2005. Wind-driven barotropic circulation off Newfoundland and labrador. Continent. Shelf Res. 25, 2084–2106. https://doi.org/10.1016/j.csr.2005.04.015.
Han, G., Lu, Z., Wang, Z., Helbig, J., Chen, N., de Young, B., 2008. Seasonal variability of the labrador current and shelf circulation off Newfoundland. J. Geophys. Res. 113, C10013 https://doi.org/10.1029/2007JC004376.
Han, G., Ohashi, K., Chen, N., Myers, P.G., Nunes, N., Fischer, J., 2010. Decline and partial rebound of the Labrador Current 1993–2004: monitoring ocean currents from altimetric and conductivity-temperature-depth data. J. Geophys. Res. 115, C12012 https://doi.org/10.1029/2009JC006091.
Harrison, W.G., Li, W.K.W., 2008. Phytoplankton growth and regulation in the Labrador Sea: light and nutrient limitation. J. Northwest Atl. Fish. Sci. 39, 71–82. https://doi.org/10.2960/J.v39.m592.
Harrison, W.G., Yngve Børsheim, K., Li, W.K.W., Maillet, G.L., Pepin, P., Sakshaug, E., Skogen, M.D., Yeats, P.A., 2013. Phytoplankton production and growth regulation in the Subarctic North Atlantic: a comparative study of the Labrador Sea-Labrador/Newfoundland shelves and Barents/Norwegian/Greenland seas and shelves. Prog. Oceanogr. 114, 26–45. https://doi.org/10.1016/j.pocean.2013.05.003.
Hatch, M.B.A., Schellenberg, S.A., Carter, M.L., 2013. Ba/Ca variations in the modern intertidal bean clam *Donax gouldii*: an upwelling proxy? Palaeogeogr. Palaeoclimatol. Palaeoecol. 373, 98–107. https://doi.org/10.1016/j.palaeo.2012.03.006.
Hellstrom, J., Paton, C., Woodhead, J., Hergt, J., 2008. Iolite: software for spatially resolved LA-(quad and MC) ICPMS analysis. Mineral. Assoc. Canada Short Course Ser. 40, 343–348.
Henson, S.A., Dunne, J.P., Sarmiento, J.L., 2009. Decadal variability in North Atlantic phytoplankton blooms. J. Geophys. Res. 114, C04013 https://doi.org/10.1029/2008JC005139.
Hetzinger, S., Halfar, J., Zack, T., Mecking, J.V., Kunz, B.E., Jacob, D.E., Adey, W.H., 2013. Coralline algal Barium as indicator for 20th century northwestern North Atlantic surface ocean freshwater variability. Sci. Rep. 3, 1761. https://doi.org/10.1038/srep01761.
Hovis, W.A., Clark, D.K., Anderson, F., Austin, R.W., Wilson, W.H., Baker, E.T., Ball, D., Gordon, H.R., Mueller, J.L., El-sayed, S.Z., Sturm, B., Wrigley, R.C., Yentsch, C.S., 1980. Nimbus-7 coastal zone color scanner: system description and initial imagery. Science 210, 60–63. https://doi.org/10.1126/science.210.4465.60 (80-.).
Hurrell, J.W., Deser, C., 2010. North Atlantic climate variability: the role of the north Atlantic oscillation. J. Mar. Syst. 79, 231–244. https://doi.org/10.1016/j.jmarsys.2009.11.002.
Jochum, K.P., Weis, U., Stoll, B., Kuzmin, D., Yang, Q., Raczek, I., Jacob, D.E., Stracke, A., Birbaum, K., Frick, D.A., Günther, D., Enzweiler, J., 2011. Determination of reference values for NIST SRM 610-617 glasses following ISO guidelines. Geostand. Geoanal. Res. 35, 397–429. https://doi.org/10.1111/j.1751-908X.2011.00120.x.
Katz, M.E., Cramer, B.S., Franzese, A., Honisch, B., Miller, K.G., Rosenthal, Y., Wright, J. D., 2010. Traditional and emerging geochemical proxies in foraminifera. J. Foraminifer. Res. 40, 165–192. https://doi.org/10.2113/gsjfr.40.2.165.
Lacour, L., Claustre, H., Prieur, L., D'Ortenzio, F., 2015. Phytoplankton biomass cycles in the North Atlantic subpolar gyre: a similar mechanism for two different blooms in the Labrador Sea. Geophys. Res. Lett. 42, 5403–5410. https://doi.org/10.1002/2015GL064540.
Lazareth, C., Vander Putten, E., André, L., Dehairs, F., 2003. High-resolution trace element profiles in shells of the mangrove bivalve Isognomon ephippium: a record of environmental spatio-temporal variations? Estuar. Coast Shelf Sci. 57, 1103–1114. https://doi.org/10.1016/S0272-7714(03)00013-1.
Lea, D.W., 2014. Elemental and isotopic proxies of past ocean temperatures. In: Treatise on Geochemistry. Elsevier, pp. 373–397. https://doi.org/10.1016/B978-0-08-095975-7.00614-8.
Lorrain, A., Gillikin, D.P., Paulet, Y.M., Chauvaud, L., Le Mercier, A., Navez, J., André, L., 2005. Strong kinetic effects on Sr/Ca ratios in the calcitic bivalve Pecten maximus. Geology 33 (12), 965–968. https://doi.org/10.1130/G22048.1.
Lozier, M.S., 2012. Overturning in the north Atlantic. Ann. Rev. Mar. Sci. 4, 291–315. https://doi.org/10.1146/annurev-marine-120710-100740.
Marali, S., Schöne, B.R., Mertz-Kraus, R., Griffin, S.M., Wanamaker, A.D., Butler, P.G., Holland, H.A., Jochum, K.P., 2017a. Reproducibility of trace element time-series (Na/Ca, Mg/Ca, Mn/Ca, Sr/Ca, and Ba/Ca) within and between specimens of the bivalve *Arctica islandica* – a LA-ICP-MS line scan study. Palaeogeogr. Palaeoclimatol. Palaeoecol. 484, 109–128. https://doi.org/10.1016/j.palaeo.2016.11.024.
Marali, S., Schöne, B.R., Mertz-Kraus, R., Griffin, S.M., Wanamaker, A.D., Matras, U., Butler, P.G., 2017b. Ba/Ca ratios in shells of *Arctica islandica* —potential environmental proxy and crossdating tool. Palaeogeogr. Palaeoclimatol. Palaeoecol. 465, 347–361. https://doi.org/10.1016/j.palaeo.2015.12.018.
Marchese, C., Castro de la Guardia, L., Myers, P.G., Bélanger, S., 2019. Regional differences and inter-annual variability in the timing of surface phytoplankton blooms in the Labrador Sea. Ecol. Indicat. 96, 81–90. https://doi.org/10.1016/j.ecolind.2018.08.053.
Marinov, I., Doney, S.C., Lima, I.D., 2010. Response of ocean phytoplankton community structure to climate change over the 21st century: partitioning the effects of nutrients, temperature and light. Biogeosciences 7, 3941–3959. https://doi.org/10.5194/bg-7-3941-2010.
Marra, J., 2004. The compensation irradiance for phytoplankton in nature. Geophys. Res. Lett. 31 n/a-n/a. https://doi.org/10.1029/2003GL018881.
Mignot, A., Claustre, H., Uitz, J., Poteau, A., D'Ortenzio, F., Xing, X., 2014. Understanding the seasonal dynamics of phytoplankton biomass and the deep chlorophyll maximum in oligotrophic environments: a Bio-Argo float investigation. Global Biogeochem. Cycles 28, 856–876. https://doi.org/10.1002/2013GB004781.
Muzuka, A.N., Hillaire-Marcel, C., 1999. Burial rates of organic matter along the eastern Canadian margin and stable isotope constraints on its origin and diagenetic evolution. Mar. Geol. 160, 251–270. https://doi.org/10.1016/S0025-3227(99)00022-5.
Nezlin, N.P., Afanasyev, Y.D., Ginzburg, A.I., Kostianoy, A.G., 2002. Remotely sensed studies of phytoplankton dynamics under physical forcing in different ocean regions. Adv. Space Res. 29, 99–106. https://doi.org/10.1016/S0273-1177(01)00222-8.
Paillard, D., Labeyrie, L.D., Yiou, P., 1996. AnalySeries 1.0: a Macintosh software for the analysis of geophysical time-series. Eos 77, 379.
Paton, C., Hellstrom, J., Paul, B., Woodhead, J., Hergt, J., 2011. Iolite: freeware for the visualisation and processing of mass spectrometric data. J. Anal. Atomic Spectrom. 26, 2508. https://doi.org/10.1039/c1ja10172b.
Poitevin, P., Thébault, J., Schöne, B.R., Jolivet, A., Lazure, P., Chauvaud, L., 2018. Ligament, hinge, and shell cross-sections of the Atlantic surfclam (*Spisula solidissima*): promising marine environmental archives in NE North America. PloS One 13, e0199212. https://doi.org/10.1371/journal.pone.0199212.
Poitevin, P., Thébault, J., Siebert, V., Donnet, S., Archambault, P., Doré, J., Chauvaud, L., Lazure, P., 2019. Growth response of *Arctica islandica* to North Atlantic oceanographic conditions since 1850. Front. Mar. Sci. 6, 483. https://doi.org/10.3389/fmars.2019.00483.
Poulain, C., Gillikin, D.P., Thébault, J., Munaron, J.M., Bohn, M., Robert, R., Paulet, Y.-M., Lorrain, A., 2015. An evaluation of Mg/Ca, Sr/Ca, and Ba/Ca ratios as environmental proxies in aragonite bivalve shells. Chem. Geol. 396, 42–50. https://doi.org/10.1016/j.chemgeo.2014.12.019.
Prendergast, A.L., Versteegh, E.A.A., Schöne, B.R., 2017. New research on the development of high-resolution palaeoenvironmental proxies from geochemical properties of biogenic carbonates. Palaeogeogr. Palaeoclimatol. Palaeoecol. 484, 1–6. https://doi.org/10.1016/j.palaeo.2017.05.032.
Racault, M.-F., Le Quéré, C., Buitenhuis, E., Sathyendranath, S., Platt, T., 2012. Phytoplankton phenology in the global ocean. Ecol. Indicat. 14, 152–163. https://doi.org/10.1016/j.ecolind.2011.07.010.
Rahmstorf, S., Box, J.E., Feulner, G., Mann, M.E., Robinson, A., Rutherford, S., Schaffernicht, E.J., 2015. Exceptional twentieth-century slowdown in Atlantic Ocean overturning circulation. Nat. Clim. Change 5, 475–480. https://doi.org/10.1038/nclimate2554.
Rhoads, D.C., Pannella, G., 1970. The use of molluscan shell growth patterns in ecology and paleoecology. Lethaia 3, 143–161. https://doi.org/10.1111/j.1502-3931.1970.tb01854.x.
Rosenberg, G.D., 1989. The "vital effect" on skeletal trace element content as exemplified by magnesium. Skeletal Biomineralization: Patterns Proc. Evol. Trends 5, 271–281. https://doi.org/10.1029/SC005p0271.
Saba, V.S., Griffies, S.M., Anderson, W.G., Winton, M., Alexander, M.A., Delworth, T.L., Hare, J.A., Harrison, M.J., Rosati, A., Vecchi, G.A., Zhang, R., 2016. Enhanced warming of the northwest Atlantic ocean under climate change. J. Geophys. Res. Ocean 121, 118–132. https://doi.org/10.1002/2015JC011346.
Schlesinger, M.E., Ramankutty, N., 1994. An oscillation in the global climate system of period 65–70 years. Nature 367, 723.
Schöne, B.R., 2013. Arctica islandica (Bivalvia): a unique paleoenvironmental archive of the northern North Atlantic Ocean. Global Planet. Change 111, 199–225. https://doi.org/10.1016/j.gloplacha.2013.09.013.
Schöne, B.R., Surge, D.M., 2012. Part N, Revised, Volume 1, Chapter 14: bivalve sclerochronology and geochemistry. Treatise Online 46, 1–24.
Schöne, B.R., Dunca, E., Fiebig, J., Pfeiffer, M., 2005. Mutvei's solution: an ideal agent for resolving microgrowth structures of biogenic carbonates. Palaeogeogr. Palaeoclimatol. Palaeoecol. 228, 149–166. https://doi.org/10.1016/j.palaeo.2005.03.054.
Schöne, B.R., Radermacher, P., Zhang, Z., Jacob, D.E., 2013. Crystal fabrics and element impurities (Sr/Ca, Mg/Ca, and Ba/Ca) in shells of *Arctica islandica*—implications for paleoclimate reconstructions. Palaeogeogr. Palaeoclimatol. Palaeoecol. 373, 50–59. https://doi.org/10.1016/j.palaeo.2011.05.013.
Seki, O., Ikehara, M., Kawamura, K., Nakatsuka, T., Ohnishi, K., Wakatsuchi, M., Narita, H., Sakamoto, T., 2004. Reconstruction of paleoproductivity in the Sea of Okhotsk over the last 30 kyr. Paleoceanography 19 n/a-n/a. https://doi.org/10.1029/2002PA000808.
Sheng, J., 2001. Dynamics of a buoyancy-driven coastal jet: the Gaspé current. J. Phys. Oceanogr. 31, 3146–3162. https://doi.org/10.1175/1520-0485(2001)031<3146:DOABDC>2.0.CO;2.
Sherwood, O.A., Lehmann, M.F., Schubert, C.J., Scott, D.B., McCarthy, M.D., 2011. Nutrient regime shift in the western North Atlantic indicated by compound-specific 15N of deep-sea gorgonian corals. Proc. Natl. Acad. Sci. Unit. States Am. 108, 1011–1015. https://doi.org/10.1073/pnas.1004904108.
Smeed, D.A., McCarthy, G.D., Cunningham, S.A., Frajka-Williams, E., Rayner, D., Johns, W.E., Meinen, C.S., Baringer, M.O., Moat, B.I., Duchez, A., Bryden, H.L., 2014. Observed decline of the Atlantic meridional overturning circulation 2004–2012. Ocean Sci. 10, 29–38. https://doi.org/10.5194/os-10-29-2014.
Stecher, H.A., Krantz, D.E., Lord, C.J., Luther, G.W., Bock, K.W., 1996. Profiles of strontium and barium in *Mercenaria mercenaria* and *Spisula solidissima* shells. Geochem. Cosmochim. Acta 60, 3445–3456. https://doi.org/10.1016/0016-7037(96)00179-2.

Steinacher, M., Joos, F., Frölicher, T.L., Bopp, L., Cadule, P., Cocco, V., Doney, S.C., Gehlen, M., Lindsay, K., Moore, J.K., Schneider, B., Segschneider, J., 2010. Projected 21st century decrease in marine productivity: a multi-model analysis. Biogeosciences 7, 979–1005. https://doi.org/10.5194/bg-7-979-2010.

Stock, C.A., Dunne, J.P., John, J.G., 2014. Drivers of trophic amplification of ocean productivity trends in a changing climate. Biogeosciences 11, 7125–7135. https://doi.org/10.5194/bg-11-7125-2014.

Stokes, M.A., Smiley, T.L., 1968. An Introduction to Tree-Ring Dating. The University of Arizona.

Takesue, R.K., Bacon, C.R., Thompson, J.K., 2008. Influences of organic matter and calcification rate on trace elements in aragonitic estuarine bivalve shells. Geochem. Cosmochim. Acta 72, 5431–5445. https://doi.org/10.1016/j.gca.2008.09.003.

Thébault, J., Chauvaud, L., L'Helguen, S., Clavier, J., Barats, A., Jacquet, S., PÉcheyran, C., Amouroux, D., 2009. Barium and molybdenum records in bivalve shells: geochemical proxies for phytoplankton dynamics in coastal environments? Limnol. Oceanogr. 54, 1002–1014. https://doi.org/10.4319/lo.2009.54.3.1002.

Vander Putten, E., Dehairs, F., Keppens, E., Baeyens, W., 2000. High resolution distribution of trace elements in the calcite shell layer of modern mytilus edulis: environmental and biological controls. Geochem. Cosmochim. Acta 64, 997–1011. https://doi.org/10.1016/S0016-7037(99)00380-4.

Weidman, C.R., Jones, G.A., Kyger, 1994. The long-lived mollusc Arctica islandica: a new paleoceanographic tool for the reconstruction of bottom temperatures for the continental shelves of the northern North Atlantic Ocean. J. Geophys. Res. 99, 18305 https://doi.org/10.1029/94JC01882.

Wigley, T.M.L., Jones, P.D., Briffa, K.R., 1987. Cross-dating methods in dendrochronology. J. Archaeol. Sci. 14, 51–64. https://doi.org/10.1016/S0305-4403(87)80005-5.

Wu, Y., Platt, T., Tang, C., Sathyendranath, S., 2008. Regional differences in the timing of the spring bloom in the Labrador Sea. Mar. Ecol. Prog. Ser. 355, 9–20. https://doi.org/10.3354/meps07233.

Yu, L., Gao, Y., Otterå, O.H., 2016. The sensitivity of the Atlantic meridional overturning circulation to enhanced freshwater discharge along the entire, eastern and western coast of Greenland. Clim. Dynam. 46, 1351–1369. https://doi.org/10.1007/s00382-015-2651-9.

Zhai, L., Platt, T., Tang, C., Sathyendranath, S., Hernández Walls, R., 2011. Phytoplankton phenology on the scotian shelf. ICES J. Mar. Sci. 68, 781–791. https://doi.org/10.1093/icesjms/fsq175.